J. Fixed Point Theory Appl. (2022) 24:16
https://doi.org/10.1007/s11784-021-00913-w
Published online January 16, 2022

Journal of Fixed Point Theory and Applications

Periodic Cauchy problem of Heisenberg ferromagnet and its geometric framework

Hsiao-Fan Liu

Abstract. We formulate algebraically solutions to the isotropic Heisenberg ferromagnet, which is an integrable geometric curve flow. The derivation is based on correspondences between this Heisenberg ferromagnet and the nonlinear Schrödinger equation. The existence of solutions to the Cauchy problems of the isotropic Heisenberg ferromagnet with periodic boundary conditions follows from the correspondence. We then obtain a geometric framework of algorithms to solve the periodic Cauchy problem numerically for the Heisenberg ferromagnet. Analytical and experimental results will be presented.

Mathematics Subject Classification. Primary 14H70, 17B80, 53-04, 68U20.

Keywords. Heisenberg ferromagnet, vortex filament equation, nonlinear Schrödinger equation, implicit spectral method.

1. Introduction

The isotropic Heisenberg ferromagnet is defined by

$$\gamma_t = \gamma \times \gamma_{xx}, \tag{1.1}$$

where $\gamma(x,t)$ is a real-valued vector function of $\mathbb{S}^2$ on $(x,t) \in \mathbb{R} \times [0,\infty)$, and $\times$ is the cross product in $\mathbb{R}^3$. It has been attracting mathematicians' and physicists' attention for decades. Takhtajan [1] first applied the inverse scattering method to describe its solution scheme. Tjon and Wright in [2] studied solitons of (1.1) in one dimension for the isotropic and anisotropic cases. Most interestingly, it has been possible to solve the arbitrary initial value problem exactly since the equation of motion is completely integrable [3].

It is well-known that (1.1) is related to the cubic non-linear Schrödinger equation (NLS)

$$q_t = i(q_{xx} + 2|q|^2 q). \tag{1.2}$$

This work was completed under the support of the MOST research grant 108-2115-M-032-008-MY2.

The relation between (1.1) and (1.2) has been discussed by Zakharov and Takhtadzhyan in [4,5], where (1.1) is known as the isotropic Heisenberg ferromagnet, and by Terng and Uhlenbeck in [6], where (1.1) is one of the Schrödinger flows on Grassmannians. For this reason, we also say that $\gamma(x,t)$ satisfying (1.1) is a *Schrödinger curve*.

Another well-known curve flow relevant to (1.2) is the vortex filament equation (VFE) in $\mathbb{R}^3$ defined by

$$\alpha_t = \alpha_x \times \alpha_{xx}, \tag{1.3}$$

which models the movement of a thin vortex in a viscous fluid and preserves the arc length parameter. Suppose we parametrize $\alpha(\cdot,t)$ by its arc length. Then Hasimoto transform in [7] relates solutions $\alpha(\cdot,t)$ of (1.3) to that of (1.2) via

$$q(x,t) = k(x,t)e^{i(\theta(t)+\int_0^x \tau(s,t)\mathrm{d}s)}, \tag{1.4}$$

where $k(\cdot,t), \tau(\cdot,t)$ are the curvature and torsion for $\alpha(\cdot,t)$, respectively, and $q(x,t)$ is a solution of NLS. Numerical solutions of VFE have been studied for years. Hou *et al.* generalized the $\theta - L$ formulation [8] to compute the motion of the curve in space numerically by considering the normal principal curvatures k_1, k_2 as new variables [9].

Numerical simulation has been an important tool in the study of dynamic issues in ferromagnetic materials [10–15]. If one differentiates a solution $\alpha(x,t)$ of (1.3) with respect to x, a Schrödinger curve is given by α_x. It is natural to obtain numerical solutions of (1.1) this way [16]. However, Terng and Uhlenbeck in [3,6] formulate the correspondences between NLS, VFE, and the Schrödinger flow on $\mathbb{S}^2$ using geometry. In fact, they systematically construct solutions of such curve flows by making use of Lax pairs of NLS and Lie theory. This construction of solutions to a geometric curve flow, if found, leads to a geometric framework to obtain numerical solutions to a curve flow. Namely, this approach gives rise to both analytic and numerical solutions of Schrödinger flow directly.

The geometric framework suggests the following advantages. Firstly, highly nonlinear curve PDEs are reduced to integrable partial differential equations and linear ODE systems. As one of the most famous integrable PDEs, the NLS can be solved and computed numerically using various methods. In fact, the pseudospectral algorithm is one of the great tools to solve periodic Cauchy problems. Such a method is shown to converge by fixed point theorems and exhibits excellent speed and stability [17–19]. In addition, it is very simple to implement so that one has numerical periodic solutions to (3.15). With the aid of the fixed point theory, the more precise information on the right-hand side of (3.16), the fewer errors or deviations occur while solving (3.16) numerically.

Secondly, there are conservation properties since the NLS has soliton solutions. For instance, suppose γ is a solution to (1.1). We now consider the energy structure. Let $\mathcal{E}(\gamma(t)) = ||\gamma_x(t)||^2_{L^2}$ be the energy function. The energy is then conserved:

$$\mathcal{E}(\gamma(t)) = \mathcal{E}(\gamma(0)), \tag{1.5}$$

for any $t > 0$. It is known that there are infinitely many conservation laws for NLS, and hence, one can observe the corresponding curve motion by analyzing these conserved quantities. Finally, this geometric framework can be executed by choosing different numerical methods at each step.

The paper is organized as follows. In Sect. 2, we recall the equivalence relations from the results of Terng, Uhlenbeck, and Thorbergsson. Proofs are given since they give rise to initial data in implementation. In Sect. 3, we formulate the solution of the periodic Cauchy problem of (1.1) with a closed initial curve given. In Sect. 4, we give steps of our geometric framework and one practical algorithm. Issues coming from implementing, error estimates for a stationary solution, and numerical examples of periodic solutions with the Viviani's curve and spherical sinusoid as initial curves are exhibited to demonstrate the behaviors of Schrödinger curves. The discussions about error estimates are also provided, and the concluding remarks follow in Sect. 5.

2. Equivalence of the Schrödinger flow on Hermitian symmetric spaces and the NLS

Suppose (M, J, g, w) is a compact Kähler manifold with a complex structure J, the Riemannian metric g, and a symplectic form w on M satisfying $w(X, Y) = g(JX, Y)$. The *Schrödinger flow* on M (cf. [20]) is the evolution equation on $C^\infty(\mathbb{R}, M)$:

$$\gamma_t = J_\gamma(\nabla_{\gamma_x}\gamma_x), \tag{2.1}$$

where ∇ is the Levi–Civita connection of the metric g. When $M = \mathbb{C}^n$, (2.1) is the linear Schrödinger equation $\gamma_t = i\gamma_{xx}$. When $M = \mathbb{S}^2$, (2.1) gives us the Heisenberg ferromagnetic model for $\gamma : \mathbb{R}^2 \to \mathbb{S}^2$. Indeed, the complex structure of $\mathbb{S}^2$ at γ sends v to $\gamma \times v$ on $T\mathbb{S}^2_\gamma$, where $\times$ is the cross product in $\mathbb{R}^3$. Then

$$\gamma \times \nabla_{\gamma_x}\gamma_x = \gamma \times \gamma^T_{xx} = \gamma \times (\gamma_{xx} - (\gamma_{xx}, \gamma)\gamma) = \gamma \times \gamma_{xx}, \tag{2.2}$$

which obviously is the evolution (1.1) on $\mathbb{S}^2$.

The Schrödinger flow (2.1) is a Hamiltonian equation for the energy functional on $C^\infty(\mathbb{S}^1, M)$ with respect to an induced symplectic form by ω on $C^\infty(\mathbb{S}^1, M)$ (cf. [20]). Note that the critical points of the energy functional are geodesics of (M, g), so the stationary solutions of the Schrödinger flow on M are closed geodesics of M. Furthermore if M is a Hermitian symmetric space, then (2.1) can be written in terms of the Lie bracket.

To be more precise, let G be a simple complex Lie group, and τ the involution that gives the maximal compact subgroup U. It is known that there exists $a \in \mathcal{U}$ such that $\mathrm{ad(a)}^2|_{\mathcal{P}} = -\mathrm{Id}_{\mathcal{P}}$ and $\mathcal{U} = \mathcal{K} \oplus \mathcal{P}$, where $\mathcal{K}$ is the centralizer of a in $\mathcal{U}$ and $\mathcal{P}$ is the orthogonal complement of $\mathcal{K}$. Then the Adjoint U-orbit at a in $\mathcal{U}$ is diffeomorphic to U and is a compact irreducible Hermitian $\frac{U}{K}$ symmetric space.

We briefly review some results on the Schrödinger flow proved by Terng and Uhlenbeck in [6] for $\frac{U}{K} = \mathrm{Gr(k, \mathbb{C}^n)}$ and by Terng and Thorbergsson in [20] for the other three classical Hermitian symmetric spaces.

Proposition 2.1. [6,20] *Under the embedding of the Hermitian symmetric space* $\frac{U}{K}$ *as the Adjoint orbit* $U \cdot a$ *in* $\mathcal{U}$*, the Schrödinger flow on* $\frac{U}{K}$ *is*

$$\gamma_t = [\gamma, \gamma_{xx}]. \tag{2.3}$$

A Lax pair for (2.3) is also derived and proved to be gauge equivalent to a Lax pair of NLS by Terng and Uhlenbeck [6]. Proposition 2.1 implies that if M is a Hermitian symmetric space, then two evolutions, (2.1) and (2.3), are equivalent. In particular, we have $\gamma_t = [\gamma, \gamma_{xx}] = \gamma \times \gamma_{xx}$ for $M = \mathbb{S}^2$.

Theorems 2.2 and 2.3 show the construction of NLS solutions from solutions of the Schrödinger flow and vice versa. We give proof since the approach will be used later in coding.

Theorem 2.2. [20,21] *Let* $\gamma : \mathbb{R}^2 \to \frac{U}{K}$ *be a solution of the Schrödinger flow on the Hermitian symmetric space* $\frac{U}{K} = U \cdot a \subset \mathcal{U}$*. Then there exists* $g : \mathbb{R}^2 \to U$ *satisfying*

(i) $\gamma = gag^{-1}$,
(ii) $u = g^{-1}g_x : \mathbb{R}^2 \to \mathcal{U}_a^{\perp}$ *solves the* $\frac{U}{K}$*-NLS equation:*

$$u_t = [a, u_{xx}] - \frac{1}{2}[u, [u, [a, u]]], \tag{2.4}$$

(iii) $g^{-1}g_t = [a, u_x] - \frac{1}{2}[u, [a, u]]$.

Moreover, $\tilde{g}$ *satisfies (i) and (ii) if and only if there is a constant* $C \in U_a$ *such that* $\tilde{g} = gC$.

Proof. We recall that $K = U_a, P = U_a^{\perp}$ and $\mathcal{U} = \mathcal{K} \oplus \mathcal{P}$. Suppose $\gamma(x,t)$ is a solution of (2.3). Then there exists $h : \mathbb{R}^2 \to U$ such that $\gamma(x,t) = h(x,t)ah(x,t)^{-1}$. Let π_0, π_1 be orthogonal projections of $\mathcal{U}$ onto $\mathcal{K}, \mathcal{P}$, respectively. We choose $k : \mathbb{R}^2 \to K$ such that $k_x k^{-1} = -\pi_0(h^{-1}h_x)$. Set $f(x,t) = h(x,t)k(x,t)$, then $\gamma = faf^{-1}$. Moreover,

$$f^{-1}f_x = (hk)^{-1}(hk)_x = k^{-1}\pi_1(h^{-1}h_x)k \in \mathcal{P}. \tag{2.5}$$

A direct computation shows that

$$\gamma_x = f[f^{-1}f_x, a]f^{-1} = f[u, a]f^{-1} \text{ and } [\gamma, \gamma_x] = fuf^{-1}.$$

Since $\tau_\lambda = \gamma\lambda \mathrm{d}x + (\gamma\lambda^2 + [\gamma, \gamma_x]\lambda)\mathrm{d}t$ is flat for all $\lambda \in \mathbb{C}$, $f * \tau_\lambda$ is flat, i.e. the following connection is flat for all $\lambda \in \mathbb{C}$:

$$f^{-1}\tau_\lambda f + f^{-1}\mathrm{d}f = (a\lambda + u)\mathrm{d}x + (a\lambda^2 + u\lambda + f^{-1}f_t)\mathrm{d}t. \tag{2.6}$$

Therefore, $(a\lambda^2 + u\lambda + f^{-1}f_t)_x - (a\lambda + u)_t + [a\lambda + u, f^{-1}f_t] = 0$.

$$u_x + [a, f^{-1}f_t] = 0 \tag{2.7}$$

$$(f^{-1}f_t)_x - u_t + [u, f^{-1}f_t] = 0. \tag{2.8}$$

Write

$$f^{-1}f_t = P + T,$$

where $P \in \mathcal{P}$ and $T \in \mathcal{K}$, respectively. From (2.7), we have

$$P = [a, u_x],\ T_x = -\frac{1}{2}[u, [a, u]]_x. \tag{2.9}$$

So, $T = -\frac{1}{2}[u,[a,u]] + c(t)$ for some function $c(t)$.

Define $g = fy(t)$, where $y(t) \in \mathcal{K}$ such that $y_t y^{-1} = -c(t)$.

Next, we will show that g defined above satisfies the conditions $(i)-(iii)$. Since $y(t)$ and a commute, it is easy to see that $gag^{-1} = \gamma$. In particular,

$$g^{-1}g_x = y^{-1}f^{-1}f_x y = y^{-1}uy \in \mathcal{P}, \tag{2.10}$$

$$g^{-1}g_t = y^{-1}(f^{-1}f_t + y_t y^{-1})y = -\frac{1}{2}[y^{-1}uy, [a, y^{-1}uy]], \tag{2.11}$$

which means $y^{-1}uy$ is a solution of (2.4).

For the uniqueness, suppose $\tilde{g}$ satisfies $(1)-(2)$, and set $C = g^{-1}\tilde{g}$. Then

$$\tilde{g}^{-1}\tilde{g}_x = C^{-1}g^{-1}g_x C + C^{-1}C_x. \tag{2.12}$$

Since $\tilde{g}^{-1}\tilde{g}_x$ and $C^{-1}g^{-1}g_x C$ are in $\mathcal{P}$ while $C^{-1}C_x \in \mathcal{K}$,

$$C^{-1}C_x = 0. \tag{2.13}$$

Similarly, $C^{-1}C_t = 0$. So C is constant.

□

The converse is also true.

Theorem 2.3. [20,21] *Let $u : \mathbb{R}^2 \to \mathcal{U}_a^{\perp}$ be a smooth solution of (2.4). Then given any $c_0 \in U$, the following linear system for $g : \mathbb{R}^2 \to U$,*

$$\begin{cases} g^{-1}g_x = u, \\ g^{-1}g_t = [a, u_x] - \frac{1}{2}[u,[a,u]], \\ g(0,0) = c_0 \end{cases} \tag{2.14}$$

has a unique smooth solution $g : \mathbb{R}^2 \to U$. Moreover, $\gamma(x,t) = g(x,t)ag(x,t)^{-1}$ is a solution of the Schrödinger flow (2.3) on $\frac{U}{K}$.

In fact, when $\lambda = \lambda_0$ is any arbitrary real number, a shift of $\gamma = gag^{-1}$ by $2\lambda_0$ is also a solution of (2.3).

Proposition 2.4. *Let $u : \mathbb{R}^2 \to \mathcal{U}_a^{\perp}$ be a solution of (2.4) and E satisfy*

$$\begin{cases} E^{-1}E_x = a\lambda + u, \\ E^{-1}E_t = a\lambda^2 + u\lambda + [a, u_x] - \frac{1}{2}[u,[a,u]]. \end{cases} \tag{2.15}$$

If $\lambda_0 \in \mathbb{R}$ and $g(x,t) = E(x,t,\lambda_0)$, then $\gamma = gag^{-1}(x - 2\lambda_0 t, t)$ is a solution of (2.3).

Proof. Let $\eta(x,t) = gag^{-1}(x,t)$ and denote $Q_{-1} = [a, u_x] - \frac{1}{2}[u,[a,u]]$. It can be checked that

$$\begin{aligned} \eta_x &= g[u,a]g^{-1}, \\ \eta_t &= g[u\lambda_0 + Q_{-1}, a]g^{-1}. \end{aligned} \tag{2.16}$$

Direct computations show that

$$\gamma_{xx} = g[a\lambda_0 + u, [u,a]]g^{-1} + g[u_x, a]g^{-1}, \tag{2.17}$$

and therefore we obtain

$$\gamma \times \gamma_{xx} = g[a, u\lambda_0]g^{-1} + gu_x g^{-1}. \tag{2.18}$$

We see that $\gamma_t = -2\lambda_0\eta_x + \eta_t$, which gives

$$g[-u\lambda_0, a]g^{-1} + g[Q_{-1}, a]g^{-1}. \tag{2.19}$$

Here, since $[Q_{-1}, a] = u_x$, $\gamma_t = [\gamma, \gamma_{xx}]$. □

We say E is a frame of solution u if E is a solution of the ODE system (2.15).

Remark 2.5. Consider $\gamma(x,t)$ to be a great circle on the unit sphere, i.e., $\gamma(x,t) = (\cos x, \sin x, 0)$. It is obviously a solution to (2.3). Following from the proof of Theorem 2.2, one local invariant $q(x,t)$ is given by

$$q(x,t) = \frac{i}{2}e^{\frac{i}{2}t}, \tag{2.20}$$

that of course can be checked to solve the NLS.

Soliton solutions of the Schrödinger equation have been widely studied in mathematics and physics. One can compute soliton solutions using explicit formulations that are known. In fact, Bäcklund transformation gives N-soliton solutions for integrable systems, especially for the NLS.

Theorem 2.6. (Bäcklund transformation [25]) *Let $E(x,t,\lambda)$ be a frame of a solution u of the NLS (1.2), $\alpha \in \mathbb{C} \setminus \mathbb{R}$, and π a Hermitian projection of $\mathbb{C}^2$ onto V. Define*

$$k_{\alpha,\pi}(\lambda) = \mathrm{I_n} + \frac{\alpha - \bar{\alpha}}{\lambda - \alpha}\pi^{\perp}. \tag{2.21}$$

Let $\tilde{\pi}(x,t)$ be the Hermitian projection of $\mathbb{C}^2$ onto $\tilde{V}(x,t) = E(x,t,\alpha)^{-1}V$. Then we have

$$\tilde{u} = u + (\alpha - \bar{\alpha})[a, \tilde{\pi}] \tag{2.22}$$

is a solution of the NLS and

$$\tilde{E}(x,t,\lambda) = k_{\alpha,\pi}(\lambda)E(x,t,\lambda)k^{-1}_{\alpha,\tilde{\pi}(x,t)} \tag{2.23}$$

is a frame of $\tilde{u}$.

3. Main results

The correspondence discussed in Theorems 2.2 and 2.3 gives a systematic way to construct solutions of the Schrödinger flow, and hence the initial value problem of the Schrödinger flow can be solved. In this section, we focus on the sphere case, in particular, we consider the periodic Cauchy problem. Namely, given a closed curve $\gamma_0(x)$ on a unit sphere, we show the existence of a L-periodic curve that evolves according to the Heisenberg ferromagnet (1.1) and write down the algebraic solution formula explicitly. Without loss of generality, we assume that the period L is 2π for the rest of the article. The main theorem is the following.

Theorem 3.1. *For any smooth closed curve $\gamma_0(x) : [0, 2\pi] \to \mathbb{S}^2$ with period 2π, there exists a unique x-periodic $\gamma(x,t)$ with period 2π satisfying*

$$\begin{cases} \gamma_t = \gamma \times \gamma_{xx} \\ \gamma(x,0) = \gamma_0(x) \end{cases}. \tag{3.1}$$

We first note that Theorem 3.1 is a special case of Theorems 2.2 and 2.3. Theorem 2.2 shows that, for any arbitrary $\gamma_0(x) : [0, 2\pi] \to \mathbb{S}^2$ given, there is a *frame* $f : \mathbb{R} \to SU(2)$ such that $\gamma_0 = faf^{-1}$, where $a = \mathrm{diag}(\frac{\mathrm{i}}{2}, -\frac{\mathrm{i}}{2})$, satisfying $f(0) = \mathrm{I}_2$ and $f^{-1}f_x = u_0$, where u_0 is of the form

$$u_0 = \begin{pmatrix} 0 & q_0 \\ -\bar{q_0} & 0 \end{pmatrix}. \tag{3.2}$$

We notice that $f(x)$ found may not be periodic, so the essential idea is to find a periodic one. Below we show how to construct a periodic frame of γ_0.

Since γ_0 is periodic, $\gamma_0(2\pi) = \gamma_0(0)$. It yields that $f(2\pi)a = af(2\pi)$. That is, $f(2\pi)$ lies in the centralizer $SU(2)_a = \{\mathrm{diag}(e^{\mathrm{i}\theta}, e^{-\mathrm{i}\theta}) | \theta \in [0, 2\pi)\}$ and hence we may write

$$f(2\pi) = e^{2\pi c_0 a}, \tag{3.3}$$

for some constant c_0. A direct computation gives the following proposition.

Proposition 3.2. *Define*

$$\tilde{f}(x) = f(x)e^{-c_0 a x}. \tag{3.4}$$

Then $\tilde{f}(x)$ has the following properties:

1. $\gamma_0 = \tilde{f}a\tilde{f}^{-1}$
2. *$\tilde{f}(x)$ is periodic in x*
3. $\tilde{f}^{-1}\tilde{f}_x = \begin{pmatrix} -\frac{i}{2}c_0 & \tilde{q_0} \\ -\bar{\tilde{q_0}} & \frac{i}{2}c_0 \end{pmatrix}$, *where* $\tilde{q_0}(x) = q_0(x)e^{ic_0 x}$.
4. *$\tilde{q_0}$ is periodic.*

Proposition 3.2 gives us a way to decompose the periodic curve γ_0 in terms of a periodic *frame* $\tilde{f}(x)$ and a local invariant $\tilde{q_0}(x)$. Here, we call c_0 the *normal holonomy*. Next, we evolve the curve according to the partial differential equation

$$\gamma_t = \gamma \times \gamma_{xx}. \tag{3.5}$$

Proposition 3.3. *Suppose $\gamma(x,t) : [0, 2\pi] \to \mathbb{S}^2$ solves (3.5) and is periodic in x with period 2π. By Theorem 2.2, there exists $f : \mathbb{R}^2 \to SU(2)$ such that $\gamma = faf^{-1}$, $f^{-1}f_x = u$, and $f^{-1}f_t = Q_{-1}$, where*

$$a = \mathrm{diag}\left(\frac{\mathrm{i}}{2}, -\frac{\mathrm{i}}{2}\right), \quad \mathrm{u} = \begin{pmatrix} 0 & q \\ -\bar{q} & 0 \end{pmatrix}, \quad \mathrm{Q}_{-1} = \frac{\mathrm{i}}{2}\begin{pmatrix} -|q|^2 & q_x \\ \bar{q}_x & |q|^2 \end{pmatrix}. \tag{3.6}$$

Define $c_0(t)$ to be a function of t satisfying

$$f^{-1}(0,t)f(2\pi,t) = e^{2\pi c_0(t)a}. \tag{3.7}$$

Then $c_0(t)$ is independent of t.

Proof. Taking t-derivative of (3.7) gives

$$\begin{aligned} e^{2\pi c_0(t)a}2\pi c_0'(t)a &= -f^{-1}(0,t)f_t(0,t)f(2\pi,t) + f^{-1}(0,t)f_t(2\pi,t) \\ &= e^{2\pi c_0(t)a}Q_{-1}(2\pi,t) - Q_{-1}(0,t)e^{2\pi c_0(t)a}. \end{aligned}$$

It is easy to see that

$$2\pi c_0'(t)a = Q_{-1}(2\pi,t) - e^{-2\pi c_0(t)a}Q_{-1}(0,t)e^{2\pi c_0(t)a}. \tag{3.8}$$

A direct computation shows

$$e^{-2\pi c_0(t)a}Q_{-1}(0,t)e^{2\pi c_0(t)a} = \frac{i}{2}\begin{pmatrix} -|q|^2 & q_x e^{-4\pi i c_0(t)} \\ \bar{q}_x e^{4\pi i c_0(t)} & |q|^2 \end{pmatrix}. \tag{3.9}$$

Note that $Q_{-1}(0,t) = Q_{-1}(2\pi,t)$. So, $c_0'(t) = 0$, as desired. □

Next, we consider the periodic Cauchy problem for NLS. Suppose that $q : \mathbb{R}^2 \to \mathbb{C}$ is a solution [1] of

$$\begin{cases} q_t = i(q_{xx} + 2|q|^2 q) \\ q(x,0) = \tilde{q_0}(x). \end{cases}, \tag{3.10}$$

Let E satisfy

$$\begin{cases} E^{-1}E_x = \begin{pmatrix} \frac{i}{2}\lambda & q \\ -\bar{q} & -\frac{i}{2}\lambda \end{pmatrix}, \\ E^{-1}E_t = \begin{pmatrix} \frac{i}{2}\lambda^2 - i|q|^2 & q\lambda + iq_x \\ -\bar{q}\lambda + i\bar{q}_x & -\frac{i}{2}\lambda^2 + i|q|^2 \end{pmatrix}, \\ E(0,0,\bar{\lambda})^* = E(0,0,\lambda)^{-1}. \end{cases} \tag{3.11}$$

Then it turns out that there is a periodic frame for a solution q of NLS periodic in x in the following proof.

Proof of Theorem 3.1. Without loss of generality, we assume $\gamma_0(0) = a$. We know that there is $f \in SU(2)$ such that $\gamma_0 = faf^{-1}$ and

$$f^{-1}f_x = \begin{pmatrix} 0 & q_0 \\ -\bar{q}_0 & 0 \end{pmatrix}. \tag{3.12}$$

Since γ_0 is periodic, $f(2\pi)$ commutes with a. So $f(2\pi) = e^{2\pi c_0 a}$ for some $c_0 \in \mathbb{R}$. Define

$$\tilde{f}(x) = f(x)e^{-c_0 ax}. \tag{3.13}$$

By Proposition 3.2, $\tilde{f}$ is periodic and $\gamma_0 = \tilde{f}a\tilde{f}^{-1}$. In particular,

$$\tilde{f}^{-1}\tilde{f}_x = \begin{pmatrix} -\frac{i}{2}c_0 & q_0(x)e^{ic_0 x} \\ -\bar{q}_0(x)e^{-ic_0 x} & \frac{i}{2}c_0 \end{pmatrix}. \tag{3.14}$$

Let $q(x,t)$ be the solution of

$$\begin{cases} q_t = i(q_{xx} + 2|q|^2 q) \\ q(x,0) = q_0(x)e^{ic_0 x} \end{cases}, \tag{3.15}$$

[1] The global smooth solution to this periodic Cauchy problem has been investigated in [22–24].

periodic in x, and $E(x,t,\lambda)$ the extended frame for q satisfying

$$\begin{cases} E^{-1}E_x = a(-c_0) + u, \\ E^{-1}E_t = ac_0^2 + u(-c_0) + Q_{-1}(u), \\ E(0,0,-c_0) = \tilde{f}(0). \end{cases} \tag{3.16}$$

We claim that $g(x,t) = E(x,t,-c_0)$ is periodic in x with period 2π. Let $y(t) = g(2\pi,t) - g(0,t)$. We know $g^{-1}g_t = c_0^2 a - c_0 u + Q_{-1}(u)$ and $u = \begin{pmatrix} 0 & q \\ -\bar{q} & 0 \end{pmatrix}$ is periodic. Then

$$\begin{aligned} y'(t) &= g(2\pi,t)(c_0^2 a - c_0 u + Q_{-1}(u))|_{x=2\pi} - g(0,t)(c_0^2 a - c_0 u + Q_{-1}(u))|_{x=0} \\ &= (g(2\pi,t) - g(0,t))(c_0^2 a - c_0 u + Q_{-1}(u))|_{x=0} \\ &= y(t)A(t), \end{aligned}$$

where $A(t) = (c_0^2 a - c_0 u + Q_{-1}(u))|_{x=0}$.

Since $y(0) = 0$ solves the ODE $y'(t) = y(t)A(t)$, the uniqueness theorem of ODE shows that $y(t) \equiv 0$. The claim follows. Let $\eta = gag^{-1}$. Then $\gamma(x,t) = \eta(x + 2c_0 t, t)$ is a solution of $\gamma_t = \gamma \times \gamma_{xx}$ by Proposition 2.4.

It remains to verify the initial condition. Note that Proposition 3.2 implies

$$\gamma(x,0) = \eta(x,0) = \tilde{f}(x)a\tilde{f}^{-1}(x) = \gamma_0(x). \tag{3.17}$$

In particular, that γ is periodic in x follows from the periodicity of $E(x,t,-c_0)$. Finally, the uniqueness of γ follows from the uniqueness of $E(x,t,-c_0)$. □

4. Algorithm and experimental results

4.1. Geometric framework and methods of implementation

Our analysis leads to the following framework to solve numerically the periodic Cauchy problem (3.1) with initial data $\gamma_0(x) : [0, 2\pi] \to \mathbb{S}^2$ being a closed curve on $\mathbb{S}^2$. In the process, we apply the fixed point techniques to solve the periodic Cauchy problem of NLS so that numerical outcomes of local invariants are more accurate. The programming steps are decomposed as follows.

Step 1. We first write γ_0 as an element in $\mathfrak{su}(2)$ and diagonalize γ_0 to find $f \in SU(2)$ such that $\gamma_0 = faf^{-1}$ and

$$f^{-1}f_x = \begin{pmatrix} 0 & q_0 \\ -\bar{q}_0 & 0 \end{pmatrix}.$$

Step 2. Compute the normal holonomy c_0 defined by (3.3), i.e., solving

$$f^{-1}(0)f(2\pi) = e^{2\pi c_0 a}.$$

This gives the initial periodic data $q_0(x)e^{ic_0 x}$ for the periodic Cauchy problem of NLS.

Step 3. We use the WGMS method in [17] (implicit spectral method) to solve the periodic Cauchy problem of NLS (3.10) with the initial data $q_0(x)e^{ic_0x}$ obtained in Step 2.

Step 4. Solve for E in the ODE system (3.16) with the right-hand side given by solutions q_{num} of (3.10) and the initial data fe^{-c_0ax}.
With such numerical local invariant q_{num} fitting in the right-hand side of (3.16), the Runge–Kutta fourth-order method suggests the following algorithm. We first integrate $E_x = EA$ numerically from the initial point $E(0, 0, -c_0)$, that is,

$$g_1 = hE(x_n, 0)A(x_n, 0), \tag{4.1}$$

$$g_2 = h\left(E(x_n, 0) + \frac{1}{2}g_1\right)\frac{(A(x_n, 0) + A(x_{n+1}, 0))}{2}, \tag{4.2}$$

$$g_3 = h\left(E(x_n, 0) + \frac{1}{2}g_2\right)\frac{(A(x_n, 0) + A(x_{n+1}, 0))}{2}, \tag{4.3}$$

$$g_4 = h(E(x_n, 0) + g_3)A(x_{n+1}, 0), \tag{4.4}$$

$$E(x_{n+1}, 0) = E(x_n, 0) + \frac{1}{6}(g_1 + 2g_2 + 2g_3 + g_4), \tag{4.5}$$

where $A = a(-c_0) + u$ calculated in terms of numerical solution q_{num} in Step 3. Now, there are grid values $E(x_n, 0)$ at $t = 0$, and hence we can iterate $E_t = EB$ from each point (x_n, t_m) to have E evaluated at (x_n, t_{m+1}):

$$k_1 = \triangle tE(x_n, t_m)B(x_n, t_m), \tag{4.6}$$

$$k_2 = \triangle t\left(E(x_n, t_m) + \frac{1}{2}k_1\right)\frac{(B(x_n, t_m) + B(x_n, t_{m+1}))}{2}, \tag{4.7}$$

$$k_3 = \triangle t\left(E(x_n, t_m) + \frac{1}{2}k_2\right)\frac{(B(x_n, t_m) + B(x_n, t_{m+1}))}{2}, \tag{4.8}$$

$$k_4 = \triangle t(E(x_n, t_m) + g_3)B(x_n, t_{m+1}), \tag{4.9}$$

$$E(x_n, t_{m+1}) = E(x_n, t_m) + \frac{1}{6}(k_1 + 2k_2 + 2k_3 + k_4), \tag{4.10}$$

where $B = ac_0^2 + u(-c_0) + Q_{-1}(u)$ calculated in terms of numerical solution q_{num} in Step 3.

Step 5. Once E is obtained, we calculate $\gamma = EaE^{-1}$ in terms of elements in $\mathfrak{su}(2)$ and then we map them back to $\mathbb{R}^3$. By Proposition 2.4 and the interpolation, the numerical solution to (3.1) is derived.

4.2. Experimental issues

The following implementation was done in Matlab. The first step can be carried out by simply diagonalizing γ_0. One can easily check that the diagonal entries are $0.5i$ and $-0.5i$, however, the function **eig**$(\cdot)$ in Matlab does not work well here. On one hand, the f in Step 1 is a function that satisfies $\gamma_0(x) = f(x)af(x)^{-1}$ at each point x. On the other hand, we plug grid points x_i's into $\gamma_0(x)$ before applying the **eig** in Matlab. This makes the **eig** function treat $\gamma_0(x_i)$'s as individual scalar matrices, and then return eigenvectors of

$\gamma_0(x_i)$ that do not obey the same function since matrices formed by eigenvectors are not unique. For this reason, we need another way to figure out the f.

Identifying $\mathbb{R}^3$ with the skew-Hermitian matrices $\mathfrak{su}(2)$, we see that $\mathfrak{su}(2)$ has a standard basis consisting of the three elements

$$a = \begin{pmatrix} \frac{i}{2} & 0 \\ 0 & -\frac{i}{2} \end{pmatrix}, b = \begin{pmatrix} 0 & \frac{1}{2} \\ -\frac{1}{2} & 0 \end{pmatrix}, \text{ and } c = \begin{pmatrix} 0 & \frac{i}{2} \\ \frac{i}{2} & 0 \end{pmatrix}, \tag{4.11}$$

and the map between elements in $\mathfrak{su}(2)$ and vectors $\gamma_0 = (r_1, r_2, r_3)$ on the sphere is

$$\gamma_0 = (r_1, r_2, r_3) \mapsto r_1 a + r_2 b + r_3 c = \begin{pmatrix} \frac{i}{2} r_1 & \frac{1}{2} r_2 + \frac{i}{2} r_3 \\ -\frac{1}{2} r_2 + \frac{i}{2} r_3 & -\frac{i}{2} r_1 \end{pmatrix}, \tag{4.12}$$

denoted by Γ_0. A standard calculation of eigenvectors for Γ_0 shows

$$F = \begin{pmatrix} \sqrt{\frac{1+r_1}{2}} & \frac{i}{\sqrt{2}} \frac{r_2 + i r_3}{\sqrt{1+r_1}} \\ \frac{i}{\sqrt{2}} \frac{r_2 - i r_3}{\sqrt{1+r_1}} & \sqrt{\frac{1+r_1}{2}} \end{pmatrix}. \tag{4.13}$$

It can be checked that $F \in SU(2)$ and such F is not unique. We make such a choice of F for the following reasons. When $r_1 = 1$, r_2 and r_3 are obviously zero, i.e., $\Gamma_0(1) = a$. This immediately implies the matrix of eigenvectors is the 2×2 identity matrix, which agrees with our formulation of F. However, when $r_1 = -1$, $\Gamma_0(-1) = -a$. The eigenvectors are

$$\begin{pmatrix} 0 & i \\ i & 0 \end{pmatrix}. \tag{4.14}$$

Besides, let $r_1 \to -1$, we have

$$\frac{r_2 + i r_3}{\sqrt{1 + r_1}} \to \sqrt{2} e^{I\theta}, \theta = \tan \frac{r_3}{r_2}. \tag{4.15}$$

The limit of F does not exist as $r_1 \to -1$, and hence, this formulation is not continuous at $r_1 = -1$. Without loss of generality, let γ_0 not pass through the point $(-1, 0, 0)$.

We also notice that $F^{-1}F_x$ might not be an off-diagonal matrix. In order to make this happen, we follow Theorem 2.2 to rotate F by a matrix K where $-K_x K^{-1}$ is equal to the diagonal terms of $F^{-1}F_x$. For instance, consider $\gamma_0(x) = (0, \cos x, \sin x)$, then

$$F(x) = \begin{pmatrix} \frac{1}{\sqrt{2}} e^{\frac{i}{2}x} & \frac{i}{\sqrt{2}} e^{\frac{i}{2}x} \\ \frac{i}{\sqrt{2}} e^{-\frac{i}{2}x} & \frac{1}{\sqrt{2}} e^{-\frac{i}{2}x} \end{pmatrix}, \quad F^{-1}F_x = \begin{pmatrix} 0 & -\frac{1}{2} \\ \frac{1}{2} & 0 \end{pmatrix}. \tag{4.16}$$

4.3. Experimental errors

A fixed point $\gamma = a$ is the trivial solution of (1.1) with the local invariant $q = 0$. Our implementation immediately shows a fixed point on the sphere if we start with $\gamma_0(x) = (1, 0, 0)$. Given the initial curve to be a circle, then the exact solution is stationary, i.e.,

$$\gamma(x, t) = (0, \cos x, \sin x). \tag{4.17}$$

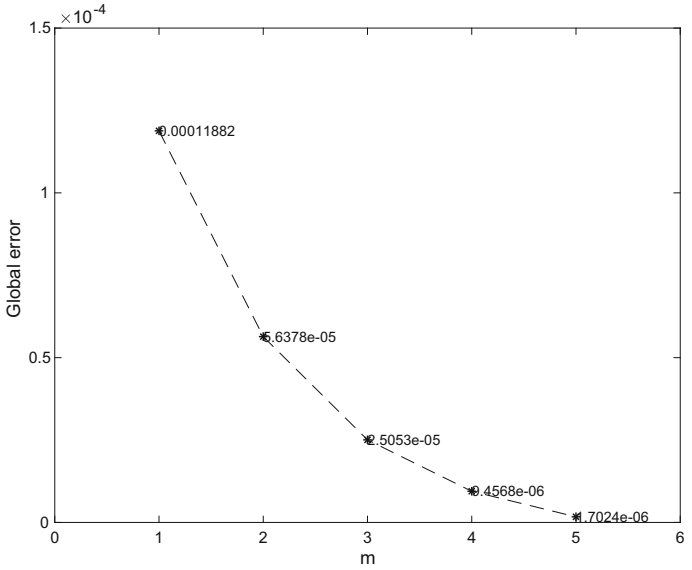

FIGURE 1. This picture shows the global error G_N^{sup} at each time step $\triangle t = \frac{10^{-3}}{2^{m-1}}$ with number of space steps $N = 2^{10}$

The corresponding invariant is $q(x,t) = -\frac{1}{2}e^{\frac{i}{2}t}$, a solution of NLS. The following errors are estimated between the numerical solution $\gamma_{\text{num}}(x,t)$ and $\gamma(x,t)$ by the L^2-norm error at each time t:

$$E_N(t) = \left(\frac{1}{N}\int_0^{2\pi} |\gamma_{\text{num}}(x,t) - \gamma(x,t)|^2 \, \mathrm{d}x\right)^{\frac{1}{2}}, \tag{4.18}$$

where N indicates the number of x partitions. The global error for different sizes of time steps is given by

$$G_N^{sup} = \max_{0 \le t_n \le T} \left(E_N^{sup}(t_n)\right), \tag{4.19}$$

where T is the total time and

$$E_N^{sup}(t) = \max_{x \in I} \left(\|\gamma_{\text{num}}(x,t) - \gamma(x,t)\|\right)$$

with $I = \{j\frac{2\pi}{N} | j = 0, 1, 2, \ldots, N-1\}$.

It is obvious that at a fixed time, the errors $E_N(t)$ are decreasing when N becomes bigger. Similarly, it is natural for us to consider how $E_N(t)$ behaves in time when N is fixed.

Figure 1 presents the global errors become around $\frac{1}{2}$ when halving the time step $\triangle t$.

As we can see in Fig. 2, the numerical energy at each time is approximately equal to the initial energy. The difference of energy at each time is less than 10^{-5} according to the left panel of Fig. 2. However, the real energy, in this case, is 2π, which is differed from the numerical energy within 0.00308

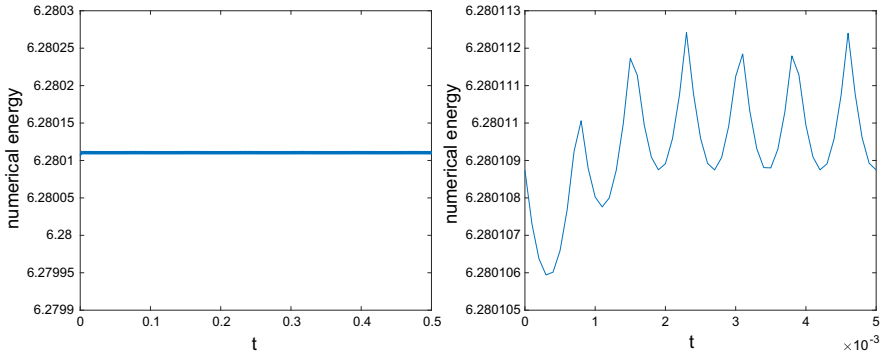

FIGURE 2. The left shows the numerical energy $\mathcal{E}(\gamma_{\text{num}}(t))$ at each time t versus the initial energy 6.28010874 at $t = 0$ with $\triangle t = 10^{-4}$, $N = 2^{12}$ and total time 0.5. The right is a zoom-in figure of the left

after 5000 time steps. The error occurs due to accumulation error of trapezoidal integration of numerical solutions $\gamma_{\text{num}}(x, t)$ and machine error. The right panel shows the errors which are controlled within 8×10^{-6}. The experimental results demonstrate this numerical energy preserving if $\triangle t$ and $\triangle x$ become smaller.

Besides the energy, the NLS has infinitely many conserved quantities. The first four conserved quantities for NLS are:

$$H_1 = \oint |q|^2 \, \mathrm{d}x, \quad H_2 = \oint \bar{q} q_x \, \mathrm{d}x, \tag{4.20}$$

$$H_3 = \oint |q_x|^2 - |q|^4 \, \mathrm{d}x, \quad H_4 = \oint q\bar{q}_x - \bar{q} q_x \, \mathrm{d}x. \tag{4.21}$$

Although one can compute the errors for these conserved quantities, it is expected that the inaccuracy will rise while calculating the integral using the trapezoidal method and the derivatives of q. Below we give some examples of numerical Heisenberg ferromagnet.

Viviani's curve

If we start with

$$\gamma_0(x) = (\sin x \cos x, \sin x, \cos^2 x),$$

which has the figure-eight shape. It is also considered to be the intersection of a sphere centered at the origin with a cylinder tangent to the sphere and passing through the origin. If one projects such curve stereographically from the point diametrically opposite the double point, then the lemniscate of Bernoulli is obtained. Figure 3 gives the motion of Schrödinger curve from $t = 0$ to $t = 3$ with time step 0.001 and $N = 2^{11}$. The bottom row in Fig. 3 consists of the behavior of corresponding local invariant q.

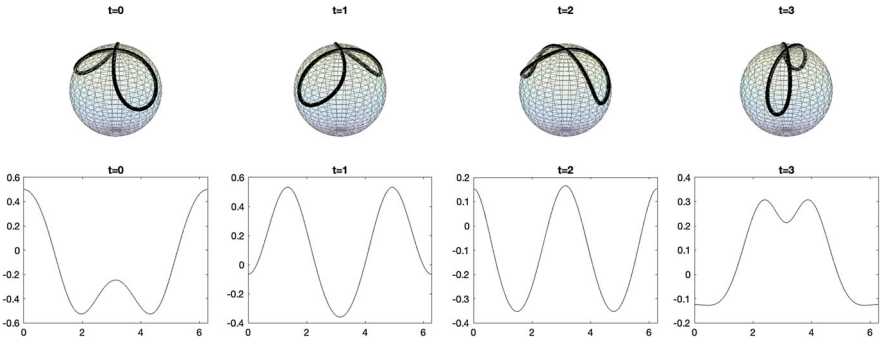

FIGURE 3. Numerical solution γ_{num} versus the real part of the corresponding local invariant q at $t = 0, 1, 2, 3$, respectively with $\triangle t = 0.001$ and $N = 2^{11}$

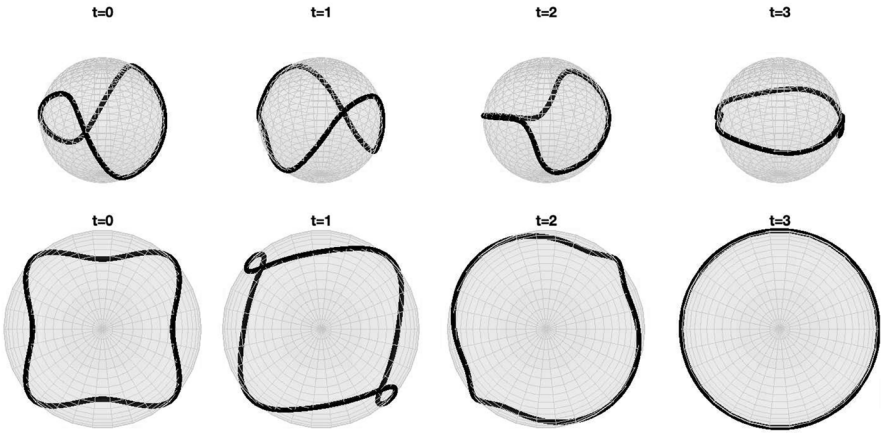

FIGURE 4. Numerical solution γ_{num} (top) versus the projection of γ_{num} onto xy plane (bottom) at $t = 0, 1, 2, 3$, respectively with $\triangle t = 0.001$

Seam line of a tennis ball

The next example is, to begin with a seam line of a tennis ball, which is an intersection of the unit sphere and the half-spherical cone. In fact, it is a case of spherical sine waves with 2 arches and the parametrized equations are

$$\gamma_0(x) = \left(\frac{\cos x}{\sqrt{1 + \cos^2 2x}}, \frac{\sin x}{\sqrt{1 + \cos^2 2x}}, \frac{\cos 2x}{\sqrt{1 + \cos^2 2x}} \right).$$

Figure 4 shows the numerical results. The top spheres consist of Schrödinger curves obtained from the initial curve $\gamma_0(x)$ with $N = 2^{11}$ and the time step 0.001 at different times, paired with those curves from an overhead viewpoint. At $t = 2$ and $t = 4$, the curves seem to have cusps only because of different perspectives. They are actually smooth.

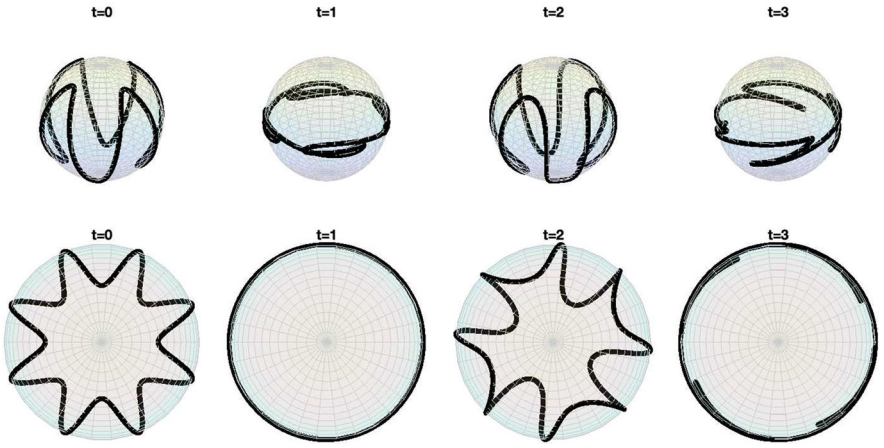

FIGURE 5. Numerical solution γ_{num} (top) for the spherical sinusoid with four arches versus the projection of γ_{num} onto xy plane (bottom) at $t = 0, 1, 2, 3$, respectively with $\triangle t = 0.001$

Spherical sinusoid with 4 arches

For simplicity and clear presentation of pictures, we consider a spherical sine wave with four arches, i.e.,

$$\gamma_0(x) = \left(\frac{\cos x}{\sqrt{1+2\cos^2 4x}}, \frac{\sin x}{\sqrt{1+2\cos^2 4x}}, \frac{\sqrt{2}\cos 4x}{\sqrt{1+2\cos^2 4x}} \right).$$

Figure 5 presents the motion of the Schrödinger curve with the initial $\gamma_0(x)$ above and it gives a better demonstration that these curves are smooth.

Schrödinger curve with 1-soliton q

Based on our geometric scheme, we are able to obtain the first periodic solution q of the NLS. Applying Bäcklund transformation to q will give us one-soliton $\tilde{q}$. Proposition 2.4 and Theorem 2.6 imply that the new $\tilde{E}(x, t, \lambda)$ will give rise to a new solution of (1.1). As an example, we apply BT on the stationary solution, i.e., a great circle. Figure 6 shows a numerical result with $\alpha = 1 - i, V = \mathbb{C}(1, i)^t$. The first picture in Fig. 6 indicates that the solution we get by applying the Bäcklund transformation is not closed. In other words, periodicity is not invariant under Bäcklund transformations. At $t = 3$, two endpoints are approaching each other. From the experimental outcomes, such a curve remains the same circle as that on the last picture in Fig. 6 until $t = 10$.

4.4. Discussion of error estimates

At a fixed time, Table 1 shows that the L^2-error $E_N(t)$ decreases when the number of grid points N is increased. Indeed, from the experimental results, we see that $\frac{E_N(t)}{E_{2N}(t)}$ is approximately 4.

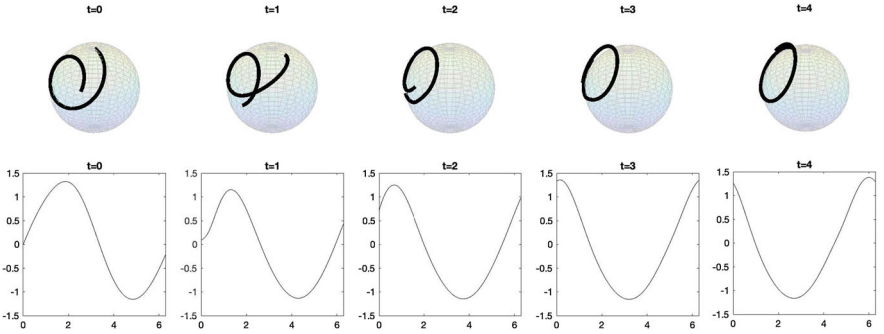

FIGURE 6. $\tilde{\gamma}_{\text{num}}$ constructed from applying BT on the circle versus the real part of the corresponding local invariant q at $t = 0, 1, 2, 3, 4$, respectively with $\triangle t = 0.01$

TABLE 1. $\triangle t = 0.001$

time steps	$E_{2^{10}}(t)$	$E_{2^{11}}(t)$	$E_{2^{12}}(t)$	$E_{2^{13}}(t)$
10	3.504E−05	8.787E−06	2.170E−06	5.347E−07
20	3.5023E−05	8.6525E−06	2.1327E−06	5.0281E−07
30	3.4701E−05	8.6484E−06	2.0757E−06	4.5323E−07
40	3.4388E−05	8.4782E−06	1.9997E−06	3.9132E−07
50	3.4400E−05	8.4270E−06	1.9061E−06	3.3050E−07
60	3.4265E−05	8.2258E−06	1.7969E−06	3.0134E−07

TABLE 2. The error G_N^{sup} computed for different $\triangle t$ with $T = 1$

N	$\triangle t = \frac{1}{1000}$	$\triangle t = \frac{1}{2000}$	$\triangle t = \frac{1}{4000}$	$\triangle t = \frac{1}{8000}$	$\triangle t = \frac{1}{16000}$
2^{10}	1.1882E−04	5.6378E−05	2.5053E−05	9.4568E−06	1.7024E−06

As for the data demonstrated in Table 2, the error G_N^{sup} becomes half of itself when we reduce time step by half with $N = 2^{10}$. The error occurs because we use the WGMS method to approximate the solution q to the NLS. Several types of numerical errors come from the WGMS algorithm, including the obvious error in approximating the integral and a truncation error when the fixed point iteration was stopped after a finite number of steps.

Another reason is that we use the Runge–Kutta fourth-order method to obtain numerical results for the frame E in (3.16) with the right-hand side filled out with the estimated q and q_x obtained by the finite difference method. This of course produces errors. It also indicates the numerical scheme can be improved by choosing other numerical methods for each step described in subsection 4.1.

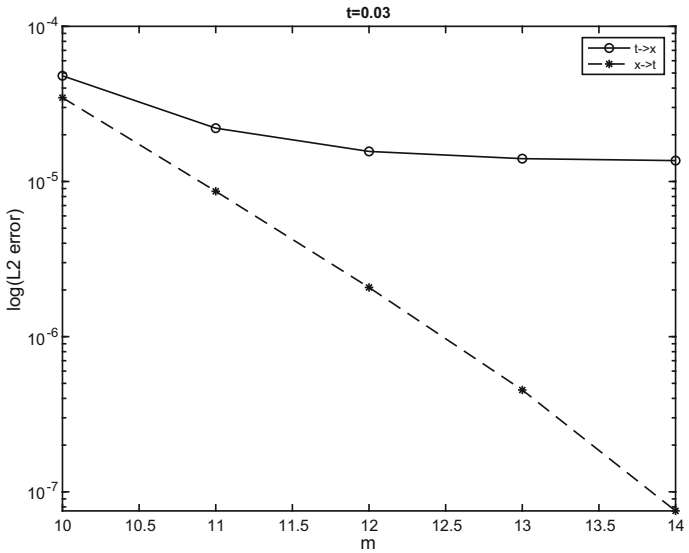

FIGURE 7. The logarithmic of L^2-error for $N = 2^m$ at $t = 0.03$, where the dashed line represents the integrating order (x, t) and the solid line represents the order (t, x)

We also note that in Step 4, the order of integrating for x and t variables does not matter theoretically when one solves for $E(x, t)$ in the ODE system. The errors presented in Table 1 come from integrating the x-direction first and then the t-direction. Below in Fig. 7, we show the comparison of L^2-errors at $t = 0.03$ according to different integrating orders of two variables x and t by the Runge–Kutta fourth-order method.

5. Concluding remarks

The geometry helps us formulate solutions to the Schrödinger flow explicitly, and our geometric framework shows that using corresponding numerical methods for each stage in the implementation can help to get numerical solutions to the nonlinear curve PDE (1.1). The advantage of this method is to transform the nonlinearity of curve motion to solve the ODE system (3.16), which makes it easier to find solutions to curve evolutions both analytically and numerically.

In addition to the Heisenberg ferromagnet, the idea of such a framework also works for the VFE despite that its formulations for curve solutions are different. As mentioned, the VFE is related to the NLS [3,7,25] and the construction of the curve is based on Sym's formula, i.e., $E_\lambda E^{-1}|_{\lambda=\lambda_0}$, provided that the principal curvature functions are given. The essential idea that we work on the ODE system instead of the nonlinear PDE has been revealed. Even though it is generally expected that this algebraic correspondence leads to a geometric framework of numerical solutions for curve motions, there are

often various technical issues while coding, such as the troublesome point $(-1, 0, 0)$ in Sect. 4.2. We will leave the discussions on technical issues in different cases to future work.

Acknowledgements

The author would like to thank Prof. Chuu-Lian Terng at University of California, Irvine, for her guidance on theoretical results. This research work is partially supported by the MOST research grant108-2115-M-032-008-MY2.

References

[1] Takhtajan, L.A.: Integration of the continuous Heisenberg spin chain through the inverse scattering method. Phys. Lett. **64A**, 235–237 (1977)

[2] Tjon, J., Wright, J.: Solitons in the continuous Heisenberg spin chain. Phys. Rev. B **15**, 17–23 (1977)

[3] Terng, C.-L.: Dispersive geometric curve flows, Surveys in Differential Geometry, vol. 19. Int. Press, Somerville (2015)

[4] Zakharov, V., Ikhailov, A.: Relativistically invariant two-dimensional models of field theory which are integrable by means of the inverse scattering problem method. Sov. Phys. JETP **74**, 1953–73 (1978)

[5] Zakharov, V., Takhtadzhyan, L.: Equivalence of the nonlinear Schrödinger equation and the equation of a Heisenberg ferromagnet. Theor. Math. Phys. **38**, 26–35 (1979)

[6] Terng, C.-L., Uhlenbeck, K.: Schrödinger flows on Grassmannians integrable systems, geometry, and topology. AMS/IP Stud. Adv. Math. **36**, 235–256 (2006)

[7] Hasimoto, H.H.: Motion of a vortex filament and its relation to elastic. J. Phys. Soc. Jpn. **31**, 293–295 (1971)

[8] Hou, T.Y., Lowengrub, J.S., Shelley, M.J.: Removing the stiffness from interfacial flows with surface tension. J. Comput. Phys. **114**, 312–338 (1994)

[9] Hou, T.Y., Klapper, I., Si, H.: Removing the stiffness of curvature in computing 3-D filaments. J. Comput. Phys. **143**, 628–664 (1998)

[10] Bertram, H.N., Seberino, C.: Numerical simulations of hysteresis in longitudinal magnetic tape. J. Magn. Magn. Mater. **193**, 388 (1999)

[11] Blue, J.L., Scheinfein, M.R.: Using multipoles decreases computation time for magnetic self-energy. IEEE Trans. Magn. **27**, 4778 (1991)

[12] Fidler, J., Schrefl, T.: Micromagnetic modelling—the current state of the art. J. Phys. D Appl. Phys. **33**, R135 (2000)

[13] Hertel, R., Kronmüller, H.: Adaptive finite element techniques in three-dimensional micromagnetics modeling. IEEE Trans. Magn. **34**, 3922 (1998)

[14] Nakatani, Y., Uesake, Y., Hayashi, N.: Direct solution of the Landau–Lifshitz–Gilbert equation for micromagnetics. Jpn. J. Appl. Phys. **28**(12), 2485 (1989)

[15] Nakatani, Y., Uesake, Y., Hayashi, N., Fukushima, H.: Computer simulation of thermal fluctuation of fine particle magnetization based on Langevin equation. J. Magn. Magn. Mater. **168**, 347 (1997)

[16] Demontis, F., Ortenzi, G., Sommacal, M.: Heisenberg ferromagnetism as an evolution of a spherical indicatrix: localized solutions and elliptic dispersionless reduction. Electron. J. Differ. Equ. **2018**(106), 1–34 (2018)

[17] Palais, R.S.: The initial value problem for weakly nonlinear PDE. J. Fixed Point Theory Appl. **16**(1–2) (2015)

[18] Forneberg, B., Whitham, G.B.: A numerical and theoretical study of certain non-linear wave phenomena. Proc. R. Soc. Lond. A **289**, 373–403 (1978)

[19] Wineberg, S.B., Gabl, E.F., Scott, L.R., Southwell, C.E.: Implicit spectral methods for wave propogation problems. J. Comput. Phys. **97**, 311–336 (1991)

[20] Terng, C.-L., Thorbergsson, G.: Completely integrable curve flows on adjoint orbits dedicated to Shiing-Shen Chern on his 90th birthday. Results Math. **40**, 286–309 (2001)

[21] Terng, C.-L., Uhlenbeck, K.: Bäcklund transformations and loop group actions. Commun. Pure Appl. Math. **53**, 1–75 (2000)

[22] Bourgain, J.: Fourier transform restriction phenomena for certain lattice subsets and applications to nonlinear evolution equations. I. Schrödinger equations. Geom. Funct. Anal. **3**(491), 107–156 (1993)

[23] Bourgain, J.: Periodic nonlinear Schrödinger equation and invariant measures. Commun. Math. Phys. **166**, 1–26 (1994)

[24] Its, A.R.: Inversion of hyperelliptic integrals, and integration of nonlinear differential equations (Russian. English summary). Vestnik Leningrad. Univ. 1976, no. 7. Mat. Meh. Astron. **2**, 39–46 (1976)

[25] Liu, H.-F., Terng, C.-L., Wu, Z:. Solitons for the Schrödinger flows on Hermitian symmetric spaces. Int. J. Math. **32**(12) (2021)

Hsiao-Fan Liu
Department of Mathematics
TamKang University
New Taipei City 25137
Taiwan, ROC
e-mail: `hfliu@mail.tku.edu.tw`

Accepted: October 23, 2021.